Magnetic phase transitions in the ternary carbides $Ln_2Cr_2C_3$ (Ln = Tb, Ho, Er)

M. Reehuis[a,b,*], K. Zeppenfeld[c], W. Jeitschko[c], N. Stüsser[b], B. Ouladdiaf[d], A. Loidl[a]

[a] *Institut für Physik, EKM, Universität Augsburg, Universitätsstr. 1, D-86159 Augsburg, Germany*
[b] *Hahn-Meitner-Institut, Glienicker Str. 100, D-14109 Berlin, Germany*
[c] *Anorganisch-Chemisches Institut, Universität Münster, Wilhelm-Klemm-Str. 8, D-48149 Münster, Germany*
[d] *Institut Laue-Langevin, BP156, F-38042 Grenoble Cedex 9, France*

1. Introduction

Systematic investigations of ternary carbides $LnTC_2$ (Ln = lanthanoid, T = V, Cr, Fe, Co, Ni, Mo, Tc, W, Re) and $Ln_2T_2C_3$ (T = Cr, Mo, Tc, W, Re) have begun more than 10 years ago [1,2]. The compounds most thoroughly studied by neutron diffraction have the compositions $LnCoC_2$ and $LnNiC_2$. Ferromagnetic order is observed for the cobalt compounds, while the nickel compounds show antiferromagnetic order of the rare earth moments [3]. Magnetization measurements of

*Corresponding author. Hahn-Meitner-Institut, Glienicker Str. 100, D-14109 Berlin, Germany. Tel.: +49-30-8062-2692; fax: +49-30-8062-2999.

E-mail address: reehuis@hmi.de (M. Reehuis).

$TbNiC_2$ and $ErNiC_2$ using single crystals revealed multistep metamagnetism [4,5]. For the carbides $DyNiC_2$ and $HoNiC_2$ commensurate–incommensurate phase transitions were found [6,7]. We have started to investigate the magnetic properties of the chromium carbides $Ln_2Cr_2C_3$ (Ln = Y, Gd–Lu) by SQUID magnetometry. Here the lanthanoid atoms show antiferromagnetism below 50 K and metamagnetic transitions up to 5.5 T [8]. The collinear antiferromagnetic structure of the compound $Dy_2Cr_2C_3$ has been determined from neutron powder diffraction data [9]. Further, we have determined the ferromagnetic structure of $Ho_2Mo_2C_3$ and $Er_2Mo_2C_3$ [10], where the crystal structure is closely related to that of $Ho_2Cr_2C_3$. In the present paper we report on the magnetic structures and phase transitions of the chromium carbides $Tb_2Cr_2C_3$, $Ho_2Cr_2C_3$ and $Er_2Cr_2C_3$. Preliminary results of this work have been presented previously [11].

2. Experimental details

Samples with a total weight of about 6 g of the carbides $Tb_2Cr_2C_3$, $Ho_2Cr_2C_3$ and $Er_2Cr_2C_3$ were prepared in an arc-melting furnace essentially as has been described earlier [2]. The starting materials were pressed to pellets, each weighting around 0.5 g and subsequently arc-melted under argon. The resulting buttons were wrapped in tantalum foil and annealed in evacuated silica tubes at 1000°Cfor 10 days. The samples were quenched in air and then ground to fine powders. The carbides were characterized by their Guinier powder patterns using Cu $K\alpha_1$ radiation. In the terbium and holmium containing samples small amounts of α-Tb_2C_3 [12] and Ho_2C[13] were detected.

The neutron powder diffraction patterns of the carbides $Tb_2Cr_2C_3$, $Ho_2Cr_2C_3$ and $Er_2Cr_2C_3$ were collected with the instrument E6 at the BER II reactor of the Hahn-Meitner-Institut in Berlin. This instrument has a double focussing graphite monochromator selecting the neutron wavelength $\lambda = 238$ pm. The data of these compounds and the temperature dependence of their magnetic peaks were measured at diffraction angles between 5° and 85°. In the case of the holmium compound additional powder patterns were recorded on the D1A instrument at the Institut Laue-Langevin in Grenoble. The data were collected at 1.6, 10, 13 and 50 K in the 2θ-range between 7° and 150°. The D1A instrument uses germanium single crystals as monochromators giving the wavelength $\lambda = 191.06$ pm.

The nuclear and magnetic structures of the investigated compounds were refined from the powder diffraction data with the program *FullProf* [14] using the nuclear scattering lengths $b(\mathrm{Tb}) = 7.38$ fm, $b(\mathrm{Ho}) = 8.08$ fm, $b(\mathrm{Er}) = 8.03$ fm, $b(\mathrm{Cr}) = 3.635$ fm and $b(\mathrm{C}) = 6.6484$ fm [15]. The magnetic form factors of the ions Tb^{3+}, Ho^{3+} and Er^{3+} were taken from Ref. [16].

3. Results and discussion

3.1. The nuclear structure of $Ho_2Cr_2C_3$

The crystal structure of the carbide $Ho_2Cr_2C_3$ (Fig. 1) was determined previously from single-crystal X-ray data [2]. The Ho, Cr and C2 atoms are on the Wyckoff position $4i(x, 0, z)$ of the space group C2/m, while the C1 atom is in $2c\,(0, 0, \frac{1}{2})$. From our present neutron powder experiment carried out on the D1A instrument we

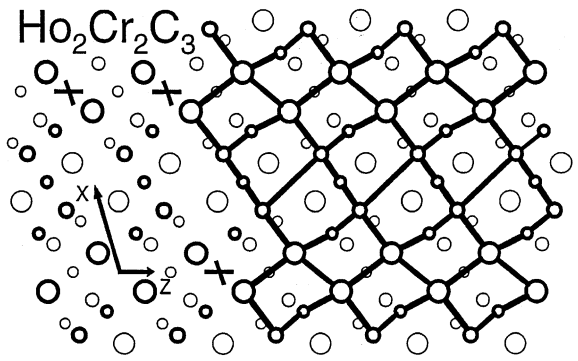

Fig. 1. The monoclinic crystal structure of $Ho_2Cr_2C_3$. The atoms connected by heavy lines are at the same heights of the projection direction. Nonconnected atoms are a half translation period above and below the connected atoms. Large, medium sized and small circles represent the lanthanoid, chromium and carbon atoms, respectively.

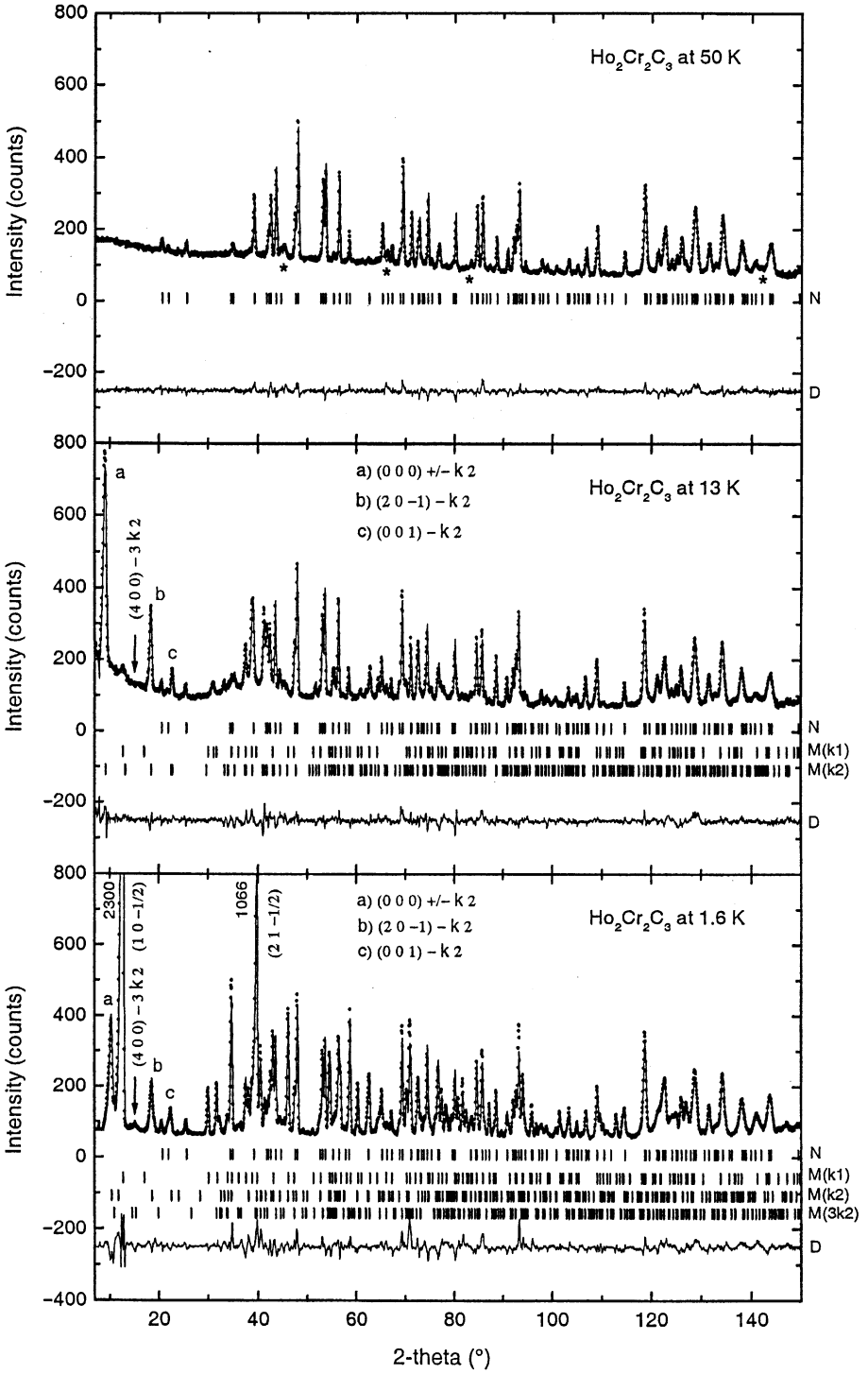

Fig. 2. Neutron diffraction patterns of $Ho_2Cr_2C_3$ ($\lambda = 191.06$ pm) collected above and below the Néel temperature. The peak positions of the nuclear (N) and magnetic (M) structures as well as the difference (D) between the observed and the calculated patterns are shown. Also shown are the strongest peaks of the impurity Ho_2C (*).

reinvestigated the crystal structure of $Ho_2Cr_2C_3$ in order to determine the positional parameters and the occupancies of the carbon atoms with a better accuracy. Just recently, a neutron diffraction study of $Er_2Mo_2C_3$ showed that its crystal structure is not completely isotypic with that of the chromium compound [10], although the space group still is the same. The only difference here arises through the differing location of the C1 atom, which was found to be on the position $2a$ $(0, 0, 0)$.

The neutron powder diffraction data of $Ho_2Cr_2C_3$ in the paramagnetic state at 50 K were used to confirm the nuclear structure (Fig. 2). The positional parameters of the atoms Ho, Cr, C(1) and C(2) obtained from the X-ray study [2] have been taken as starting values for the Rietveld refinements. A total of 20 variable parameters was refined: an overall scale factor, five peak shape parameters, the zero point, four lattice constants, six positional and three isotropic thermal parameters of the Ho, Cr and C atoms. In the last refinement the occupancies of the two carbon atoms C1 and C2 in the positions $2c$ $(0, 0, \frac{1}{2})$ and $4i(x, 0, z)$ were allowed to vary. The values occ(C1) = 0.992(16) and occ(C2) = 0.993(12) are in good agreement with the values occ(C1) = 0.98(4) and occ(C2) = 0.96(3) of the X-ray study [2]. Assuming the presence of carbon atoms in the position $2a$ $(0, 0, 0)$ as observed in $Er_2Mo_2C_3$, the refinement resulted in the value occ(C2) = 0.007(15). The nuclear structure could also be confirmed for the data sets collected at 1.6, 10 and 13 K resulting in practically the same residuals R_N (Table 1). Here the nuclear structure of $Ho_2Cr_2C_3$ was refined simultaneously with its magnetic structure, which is discussed below. The isotropic thermal parameters and the occupancies of the different atoms have been taken from the refinement of the data set at 50 K and the values were not allowed to vary. The results of the refinements are summarized in Table 1.

The $\sin\theta/\lambda$ range of the powder patterns of $Tb_2Cr_2C_3$ and $Er_2Cr_2C_3$ recorded on the E6 instrument was shorter than that of $Ho_2Cr_2C_3$ (Fig. 3). Here it seems likely that the chromium carbides $Ln_2Cr_2C_3$ (Ln = Gd–Tm) are isotypic with $Ho_2Cr_2C_3$. In order to confirm the crystal structure of $Tb_2Cr_2C_3$ and $Er_2Cr_2C_3$ we used the neutron powder data collected in the paramagnetic state at 70 and 26 K, respectively. The refinements

Table 1
Results of the Rietveld refinements of the nuclear structure of $Ho_2Cr_2C_3$ determined from neutron powder diffraction data[a]

T (K)	1.6	10	13	50	293[b]
a (pm)	1048.31(3)	1048.35(4)	1047.89(3)	1047.91(3)	1047.0(2)
b (pm)	335.434(11)	335.444(12)	335.411(9)	335.488(8)	336.50(6)
c (pm)	554.12(2)	554.11(2)	553.96(2)	553.87(1)	554.03(8)
β (°)	106.351(3)	106.353(3)	106.339(2)	106.340(2)	106.31(2)
V (nm^3)	0.18697	0.18697	0.18684	0.18685	0.18734
x(Ho)	0.3923(2)	0.3925(2)	0.3926(2)	0.3929(2)	0.39299(3)
z(Ho)	0.1812(4)	0.1809(4)	0.1815(3)	0.1809(3)	0.18347(5)
x(Cr)	0.1544(6)	0.1542(6)	0.1549(5)	0.1556(3)	0.15544(9)
z(Cr)	0.3804(11)	0.3823(12)	0.3843(9)	0.3839(6)	0.3853(2)
x(C2)	0.7188(4)	0.7191(4)	0.7179(3)	0.7188(2)	0.7161(7)
z(C2)	0.2655(6)	0.2664(6)	0.2649(4)	0.2654(3)	0.263(1)
B(Ho) (nm^3)	0.0000	0.0000	0.0000	0.0000(5)	0.00393(3)
B(Cr) (nm^3)	0.0002	0.0002	0.0002	0.0002(11)	0.0043(1)
B(C1) (nm^3)	0.0026	0.0026	0.0026	0.0026(5)	0.005(1)
B(C2) (nm^3)	0.0026	0.0026	0.0026	0.0026	0.0071(8)
R_N (no. of F's)	0.048(132)	0.049(132)	0.047(131)	0.044(131)	0.027(739)

[a] The Ho, Cr and C2 atoms are on the Wyckoff position $4i(x, 0, z)$, while the C1 atom is in $2c$ $(0, 0, \frac{1}{2})$. The isotropic thermal parameters B with the same values and the same standard deviations were constrained to be equal, those without standard deviations were not refined. R_N is the residual of the nuclear structure defined as $R_N = \sum|F_o| - |F_c|/\sum|F_o|$.

[b] For comparison the structural parameters of $Ho_2Cr_2C_3$ as determined from single-crystal X-ray data [2] are also listed.

resulted in reasonable residuals $R_N = 0.039$ and 0.074 for the terbium and erbium compound using the crystal structure parameters obtained for $Ho_2Cr_2C_3$.

3.2. *The magnetic structure of $Tb_2Cr_2C_3$*

The neutron powder patterns of $Tb_2Cr_2C_3$ collected at 1.8 K (Fig. 3) showed additional magnetic peaks, which can be ascribed to the antiferromagnetic order of the terbium sublattice. The first prominent magnetic reflections can be indexed as $(1\,0\,0)_M$, $(1\,0\,-1)_M$, $(3\,0\,0)_M$, etc. Thus, the magnetic structure violates the *C*-centering and the reflections can be generated by the rule $(h\,k\,\ell)_M = (h\,k\,\ell)_N \pm \boldsymbol{k}$, where the propagation vector is $\boldsymbol{k} = (0\,1\,0)$. The Rietveld refinements showed that the magnetic moments of the terbium atoms in the positions $(x, 0, z)$ and $(-x, 0, -z)$ are coupled antiferromagnetically. Furthermore, it could be seen that the terbium moments are aligned within the monoclinic *ac*-plane forming an angle $\varphi = 66.0(4)^\circ$ with the *a*-axis. This structure type was found earlier for the isotypic carbide $Dy_2Cr_2C_3$ [9], where the determined angle $\varphi = 65(2)^\circ$ is practically the same. The magnetic structure is presented in Fig 4. The experimental magnetic moment per terbium atom $\mu_{exp} = 8.81(10)\,\mu_B$ is close to the theoretical value $\mu_s = gJ\,\mu_B = 9.0\,\mu_B$ of the free Tb^{3+}-ion. The refinements showed further that the chromium atoms do not contribute to the magnetic order and this is in

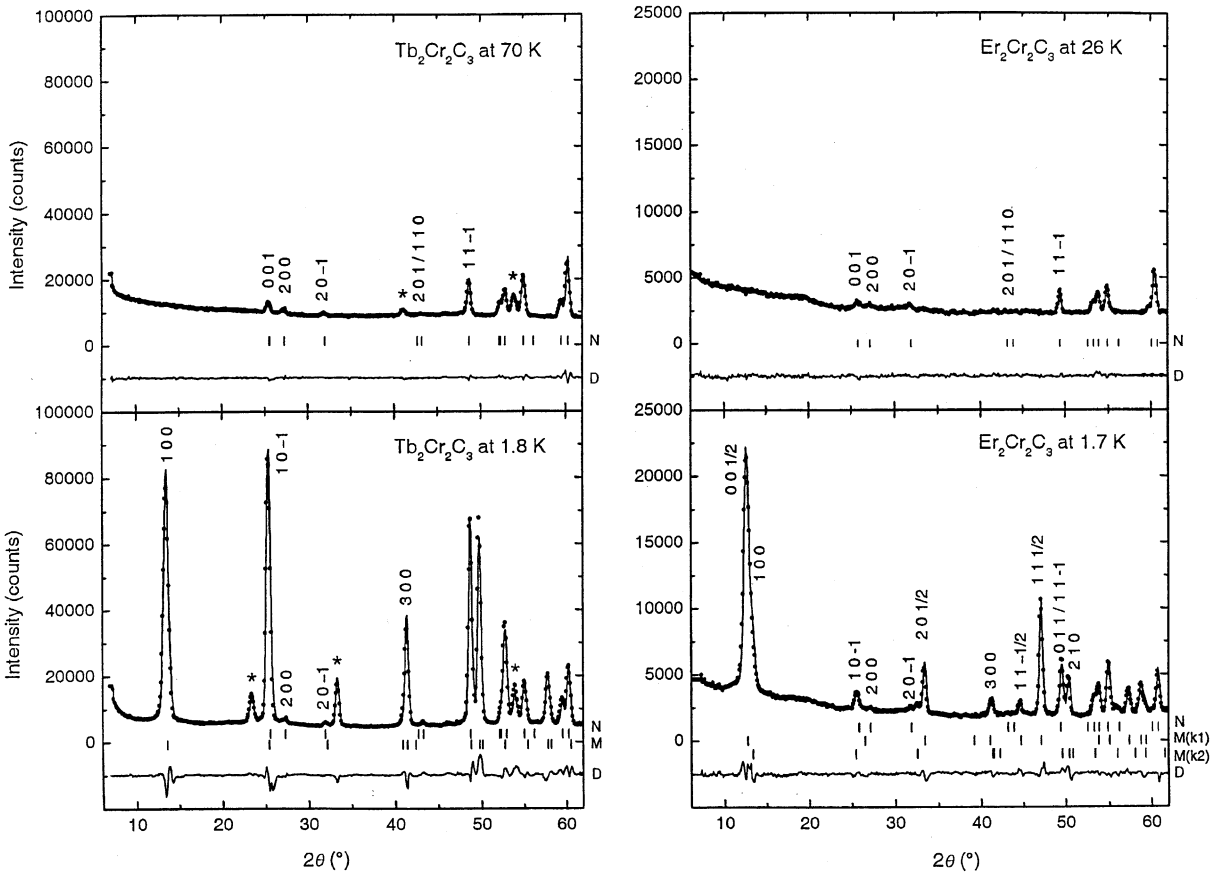

Fig. 3. Neutron diffraction patterns ($\lambda = 238$ pm) of $Tb_2Cr_2C_3$ and $Er_2Cr_2C_3$ collected above and below the Néel temperature. The peak positions of the nuclear (N) and magnetic (M) structures as well as the difference (D) between the observed and the calculated patterns are shown. Also shown are the strongest peaks of the impurity Tb_2C_3 (*).

agreement with the results of our SQUID measurements [8]. The results of the refinements are summarized in Table 2.

3.3. The magnetic structure of $Ho_2Cr_2C_3$

In contrast to the terbium carbide the magnetic behaviour of $Ho_2Cr_2C_3$ was found to be rather complex. This is already indicated by the powder pattern of $Ho_2Cr_2C_3$ recorded at 1.6 K (Fig. 2) showing an unusually large number of magnetic reflections. The two strongest magnetic peaks could be assigned with the indices $(1, 0, -\frac{1}{2})_M$ and $(2, 1, -\frac{1}{2})_M$, respectively. Thus, the magnetic unit cell requires a doubling of the monoclinic *c*-axis. The possible magnetic structure can be usually described either with the propagation vector $\boldsymbol{k} = (0, 0, \frac{1}{2})$ or with the vector $\boldsymbol{k} = (0, 1, \frac{1}{2})$. The latter one has been taken for the refinements, since the magnetic reflection $(0, 0, \frac{1}{2})_M$ is absent. Further, we assumed the same orientation of the holmium moments within the monoclinic *ac*-plane as already found for $Tb_2Cr_2C_3$ and $Dy_2Cr_2C_3$. In fact, the Rietveld refinements were successful using this model. The refined angle $\varphi = 65(2)^\circ$ between the moment direction and the *a*-axis practically is

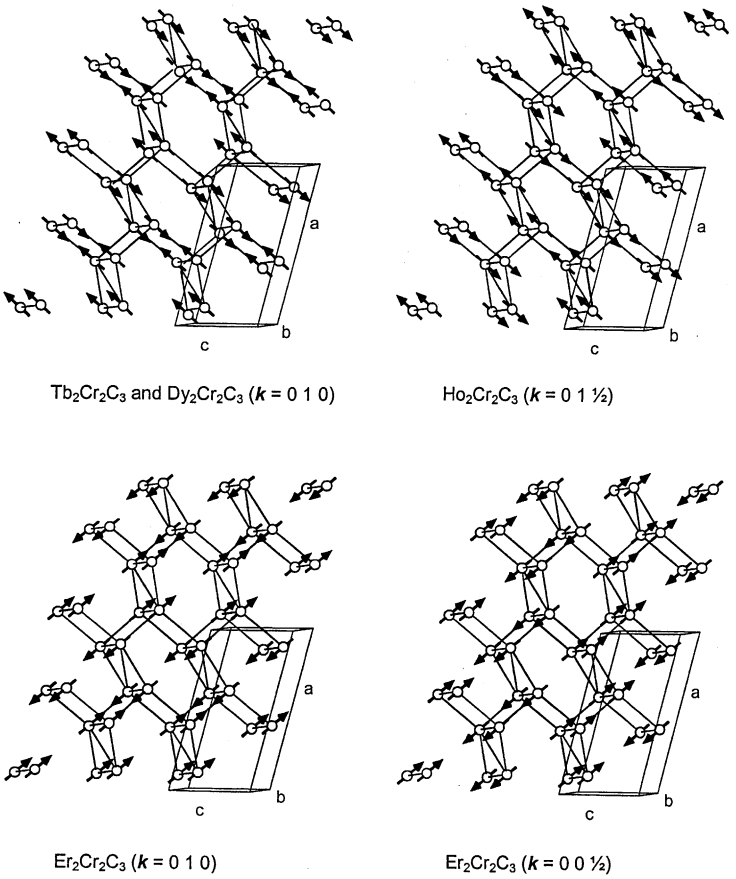

Fig. 4. The magnetic order of the lanthanoid moments in the commensurate antiferromagnetic phases of $Ln_2Cr_2C_3$ (Ln = Tb, Dy, Ho, Er). For all these compounds the magnetic moments are ordered within the monoclinic *ac*-plane. The coupling of magnetic moments of the Ln atoms along the monoclinic *b*-axis is always ferromagnetic. The coupling of a lanthanoid moment to those of the three next nearest-neighbour atoms can be ferro- or antiferromagnetic.

the same as the values $\varphi = 67.9(4)^\circ$ and $65(2)^\circ$ found for the terbium and dysprosium compounds.

After refining the magnetic structure of $Ho_2Cr_2C_3$ with the propagation vector $\boldsymbol{k}_1 = (0, 1, \frac{1}{2})$, a large number of additional magnetic peaks could not be generated using the vector $\boldsymbol{k}_1$. We were not successful in assigning indices for these magnetic reflections by using a primitive cell or cells with doubled or tripled a, b and/or c translation periods. Finally, the first strong magnetic peaks could be indexed as $(0.993, 0, -0.108)_M$, $(1.007, 0, -0.893)_M$, $(0.993, 0, -1.108)_M$, etc. Hence, a sine-wave modulated structure with the propagation vector $\boldsymbol{k}_2 = (\tau_x, 0, -\tau_z)$ was assumed. From the Rietveld refinements, we finally obtained the vector components $\tau_x = 0.9935(6)$ and $\tau_z = 0.1075(4)$. The magnetic reflections are consequently satellites of allowed nuclear peaks as $(0, 0, 0,)^{\pm}$,$(2, 0, -1)^{-}$, $(0, 0, 1)^{-}$, etc. (Fig. 2). Further it seemed likely that the magnetic ordering exhibits a square-wave modulation of the moment value propagating along the wave-vector direction. A square-wave modulated structure is established at lower temperature, when higher harmonics of fundamental satellites $(h\,k\,\ell)_M = (h\,k\,\ell)_N \pm n\boldsymbol{k}$ $(n = 3, 5, 7, \ldots)$ appear in neutron powder patterns. The magnetic moments can be calculated from the relation $n\pi/4 \times A(nk)$ $(n = 3, 5, 7, \ldots)$. In order to investigate the presence of higher harmonic peaks we simulated the powder patterns with $3\boldsymbol{k}_2$ and $5\boldsymbol{k}_2$. It could be seen that the calculated peak intensities were rather weak and only four magnetic peaks were expected to be observable in the powder pattern. Unfortunately three of these peaks were difficult to observe, since they have peak positions very similar to those of the much stronger magnetic reflections of the commensurate and incommensurate structure. Finally, only one peak $[(4, 0, 0) - 3\boldsymbol{k}_2]$ was calculated to be observable at the 2θ-position of 15.2°. In fact, at this calculated position a weak magnetic

Table 2
Results of the Rietveld refinements of the magnetic structures of $Tb_2Cr_2C_3$, $Ho_2Cr_2C_3$ and $Er_2Cr_2C_3$ as determined from neutron powder diffraction data[a]

T (K)	$Tb_2Cr_2C_3$	$Ho_2Cr_2C_3$			$Er_2Cr_2C_3$	
	1.8	1.6	10	13	1.7	5.3
a (pm)	1049.3(2)	1048.31(3)	1048.35(4)	1047.89(3)	1047.0(3)	1046.9(3)
b (pm)	340.4(1)	335.43(1)	335.44(1)	335.41(1)	333.2(1)	333.2(2)
c (pm)	560.6(2)	554.12(2)	554.11(2)	553.96(2)	550.64(2)	550.63(2)
β (°)	105.93(2)	106.351(3)	106.353(3)	106.339(2)	106.54(3)	106.53(3)
V (nm^3)	0.19255	0.18697	0.18697	0.18684	0.18414	0.18412
R_N (no. of F's)	0.050(22)	0.048(132)	0.049(132)	0.047(131)	0.065(19)	0.071(19)
$\boldsymbol{k}_1$	(0, 1, 0)	(0, 1, $\frac{1}{2}$)	(0, 1, $\frac{1}{2}$)	(0, 1, $\frac{1}{2}$)	(0, 0, $\frac{1}{2}$)	—
$\mu_{exp,1}$/Ln (μ_B)	8.82(10)	6.77(3)	6.44(3)	1.0(1)[b]	6.91(11)	—
φ_{k1} (°)	66.0(4)	67.9(4)	68.8(5)	68.8	–35.7(6)	—
$R_{M,1}$ (no. of I's)	0.055(29)	0.045(123)	0.075(123)	—	0.082(23)	—
$\boldsymbol{k}_{2,3}$	—	(τ_x, 0, $-\tau_z$)	(τ_x, 0, $-\tau_z$)	(τ_x, 0, $-\tau_z$)	(0, 1, 0)	(τ_x, 0, $\frac{1}{2} - \tau_z$)
τ_x	—	0.9935(6)	0.9930(8)	0.8856(6)	—	0.055(1)
τ_z	—	0.1075(4)	0.1120(6)	0.1395(4)	—	0.070(1)
$\mu_{exp,2}$/Ln (μ_B)	—	4.89(3)	4.71(4)	4.72(2)	4.41(7)	4.20(2)
φ_2 (°)	—	74.3(6)	72.7(6)	64.9(4)	–34.9(10)	–40(3)
$R_{M,2}$ (No. of I's)	—	0.110(253)	0.125(253)	0.090(248)	0.054(22)	0.145(19)
μ_{exp}/Ln (μ_B)	8.82(10)	8.35(5)	7.98(5)	4.82(5)	8.2(1)	4.7(1)
μ_s (μ_B)	9.0	10.0	10.0	10.0	9.0	9.0

[a] For each magnetic phase the experimental magnetic moments of the lanthanoid atoms μ_{exp} and their angles φ to the monoclinc a-axis are given. The total experimental magnetic moments μ_{exp} (calculated as $\mu^2_{exp} = \mu^2_{exp,1} + \mu^2_{exp,2}$) are compared with the theoretical values $\mu_s = gJ\,\mu_B$ of the free Ln^{3+}-ions. The residual R_M for the magnetic structure is defined as $R_M = \sum |I_o - I_c| / \sum I_o$.

[b] The holmium moment $\mu_{exp,1}$ was calculated from the intensity of the magnetic reflection (0, 1, $\frac{1}{2}$).

reflection could be found in the patterns recorded at 1.6 and 10 K. The calculated and observed intensities were in good agreement suggesting the presence of a square-wave modulated structure. In the 13 K pattern finally this peak could not be observed, and obviously this peak disappears between 10 and 13 K, exactly in that range, where the vector components τ_x and τ_z of $\boldsymbol{k}_2$ as well as the peak intensities of the incommensurate phase shift spontaneously (Figs. 5 and 6). All this indicated the presence of a phase transition from a locked-in square-wave to a sine-wave modulated structure. It is interesting to note that the refined angle $\varphi = 74.3(6)^\circ$ reveals the same orientation of the holmium moments within the *ac*-plane as found for the commensurate structure. The refinement of the magnetic structures of $Ho_2Cr_2C_3$ at 10 K showed no significant change of these magnetic structures; with the only exception that the holmium moments of both phases are slightly reduced at 10 K. This can also be seen in Figs. 5 and 6, where the temperature dependence of the magnetic intensities of some magnetic reflections is plotted.

The low-temperature powder pattern of $Ho_2Cr_2C_3$ recorded on the E6 instrument (Fig. 5) showed one additional magnetic peak at the diffraction angle $2\theta \approx 7.5^\circ$. This peak could not be generated using the propagation vectors $\boldsymbol{k}_1$ and $\boldsymbol{k}_2$. Therefore, we assumed the presence of a third magnetic phase with a propagation vector $\boldsymbol{k}_3$ with the components $\tau_x \approx \frac{1}{2}$ and $\tau_z \approx -\frac{1}{4}$. However, it has to be mentioned that the vector components can only be estimated due to the presence of just one magnetic peak. Further, it can be seen in Fig. 5 that this magnetic peak disappears at 12.5(5) K. This is exactly the same temperature, where the peaks of the commensurate phase with the propagation vector $\boldsymbol{k}_1 = (0, 1, \frac{1}{2})$ disappear. The third magnetic phase results possibly from a superimposed modulation of the commensurate phase with $\boldsymbol{k}_1$.

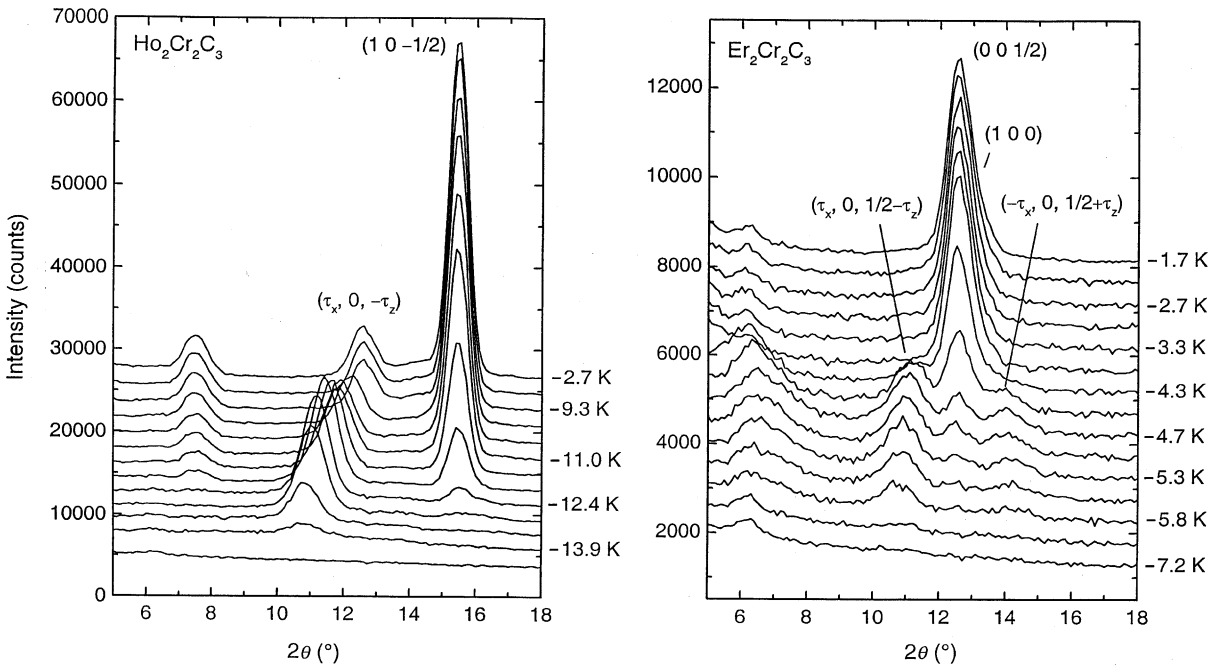

Fig. 5. Parts of the neutron powder patterns ($\lambda = 238$ pm) of $Ho_2Cr_2C_3$ and $Er_2Cr_2C_3$ between 1.7 and 15 K showing the presence magnetic phase transitions.

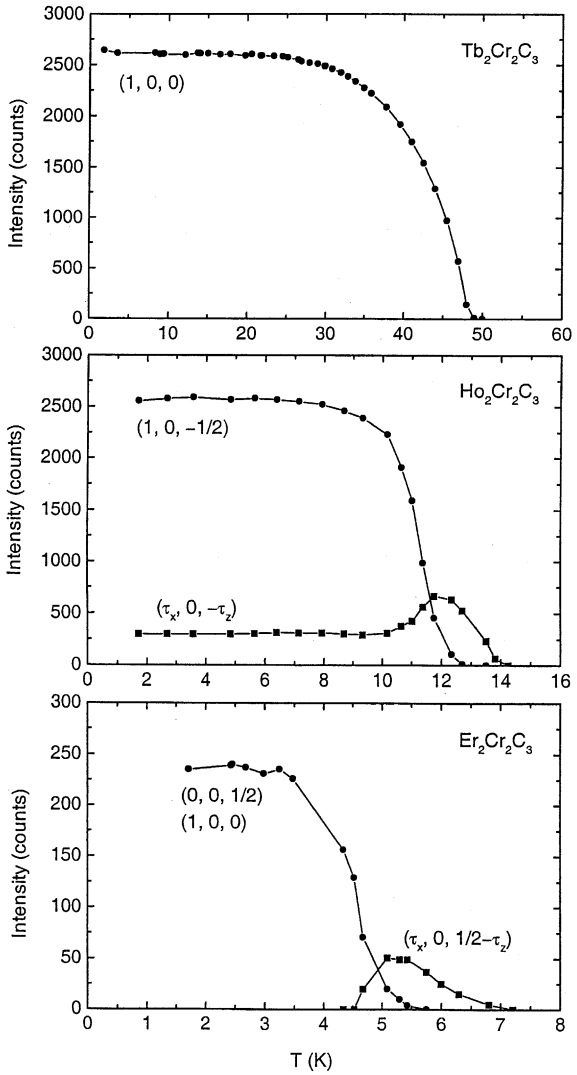

Fig. 6. Temperature dependence of the intensities of the strongest magnetic reflections for the carbides $Tb_2Cr_2C_3$, $Ho_2Cr_2C_3$ and $Er_2Cr_2C_3$.

3.4. The magnetic structure of $Er_2Cr_2C_3$

For the erbium compound two commensurate coexisting magnetic structures with the propagation vectors $\boldsymbol{k}_1 = (0\,0\,\frac{1}{2})$ and $\boldsymbol{k}_2 = (0\,1\,0)$ could be determined at 1.7 K. The refinements showed that the erbium moments are aligned within the *ac*-plane. This has been observed also for the lanthanoid sublattices in $Tb_2Cr_2C_3$, $Dy_2Cr_2C_3$ and $Ho_2Cr_2C_3$. The only difference arises from the different orientation of the moments in this plane. For both magnetic structures of the erbium carbide we obtained practically the same angles between the moment direction of the erbium atoms and the *a*-axis: $\varphi_1 = -35.7(6)^\circ$ for $\boldsymbol{k}_1$ and $\varphi_2 = -34.9(10)^\circ$ for $\boldsymbol{k}_2$. It is interesting to note that the erbium moments are approximately oriented perpendicular to those of the terbium, dysprosium and holmium atoms (Fig. 4). This may be rationalized by the different signs of the second-order terms B_2^0 of the Hamiltonian which describes the interactions of the magnetic moments with the crystalline electric fields (CEF) as found frequently in intermetallic compounds [17–19]. From both magnetic phases a total magnetic moment $\mu_{exp} = 8.12(5)\,\mu_B$ can be calculated. This moment is smaller than the theoretical value of the free Er^{3+} ion value $\mu_s = 9.0\,\mu_B$. The lower experimental moment value may be ascribed to crystal field or frustration effects.

The commensurate magnetic structures of $Er_2Cr_2C_3$ are stable up to 5.5 K (Figs. 5 and 6). In the temperature range between 4.5 and 6.8 K new magnetic peaks appear just below and above the 2θ-position of the commensurate peak $(0,0,\frac{1}{2})_M$ and $(0,1,0)_M$. Obviously, the commensurate magnetic peak $(0,0,\frac{1}{2})_M$ splits into incommensurate ones $(\tau_x,0,\frac{1}{2}-\tau_z)_M$ and $(-\tau_x,0,\frac{1}{2}+\tau_z)_M$, indicating a transition from a commensurate to an incommensurate magnetic structure with the propagation vector $\boldsymbol{k}_3 = (\tau_x,0,\frac{1}{2}-\tau_z)$. At 5.3 K the vector components were refined to be $\tau_x = 0.055(1)$ and $\tau_z = 0.070(1)$. The erbium moments were found to be in the *ac*-plane with a moment direction similar to those of the commensurate phases (Table 2).

3.5. Magnetic phase transitions

For $Tb_2Cr_2C_3$ the temperature dependence of the intensity of the magnetic reflection $(1\,0\,0)_M$ has been investigated. It can be seen in Fig. 6 that this reflection disappears at the Néel temperature $T_N = 49(1)$ K. This temperature is in good agreement with $T_N = 50(1)$ K obtained earlier from SQUID measurements [8]. The same type of magnetic order could be found earlier for

$Dy_2Cr_2C_3$ [9], where the ordering temperature $T_N = 23(1)$ K is much lower. In the case of the holmium and erbium compound the magnetic reflections disappear at the Néel temperatures $T_N = 14.0(5)$ and $6.8(5)$ K, respectively (Figs. 5 and 6). This is also in agreement with the values $T_N = 14(1)$ and $7(1)$ K obtained from SQUID measurements [8]. For both $Ho_2Cr_2C_3$ and $Er_2Cr_2C_3$, it is interesting to see that the commensurate magnetic order sets in below 12.7(3) and 5.5(3) K significantly below the Néel temperatures. A similar behaviour was also observed for the carbides $DyNiC_2$ and $HoNiC_2$ [6] as well as for the silicide $ErNiSi_2$ [20]. In $Ho_2Cr_2C_3$ the incommensurate order of the holmium moments shows a spontaneous change of the 2θ-position and the magnetic intensities at the lower temperature 10.2(2) K and they shift continuously with the temperature up to T_N. Furthermore, it is clearly evidenced that the incommensurate diffraction peak $(\tau_x, 0, -\tau_z)$ reveals a maximum close to 12 K (Fig. 6) coinciding with the onset of the commensurate phase. It is likely that the strongly increasing holmium moment of the commensurate order influences the incommensurate order in a way that the moments here are locked in spontaneously. A very similar behaviour was observed for $CePd_2Si_2$ [21]. In contrast to the holmium compound, $Er_2Cr_2C_3$ shows the onset of an incommensurate magnetic order above 4.5(2) K (Figs. 5 and 6). Thus, the commensurate and the incommensurate phases coexist in the temperature range between 4.5(2) and 5.4(2) K. The coexistence of a commensurate and incommensurate phase occurs also in the silicide $ErNiSi_2$ [20].

4. Conclusion

In spite of the complex magnetic behaviour of the investigated carbides as the presence of coexisting magnetic structures and magnetic phase transitions we could find similarities concerning the magnetic order of the lanthanoid moments. The magnetic moments of both the commensurate and incommensurate structures are aligned within the monoclinic *ac*-plane. The moment directions of the Tb, Dy and Ho atoms were found to be nearly the same. For the erbium atoms it is true that the moment direction is different, but it can be seen in Fig. 4 that the moment direction of the lanthanoid atoms is always parallel to a connection line to one of the next nearest-neighbour Ln atoms. Furthermore, the magnetic moments of the Ln atoms in all these compounds are coupled ferromagnetically along the *b*-axis, where the Ln–Ln distance is the shortest (333–340 pm). Three other Ln atoms can be found as next nearest neighbours all with slightly different and larger distances between 342 and 360 pm. As shown in Fig. 4 the coupling to these Ln atoms can be ferro- and/or antiferromagnetic. For $Er_2Cr_2C_3$ we found two coexisting magnetic phases at low temperature. The difference here arises only through the different coupling to one of the three next nearest neighbour atoms. The presence of coexisting phases may be rationalized by the fact that both the ferro- and antiferromagnetic order to those atoms which are energetically stable and they can be locked in simultaneously. On the other hand, it has to be mentioned that also a single magnetic phase can be assumed, where the two magnetic structures are superimposed. More details of the presence of coexisting phases are given in Refs. [21,22]. Different coexisting magnetic phases could be observed earlier for the intermetallic compounds as $DyNiC_2$ [6], $HoNiC_2$ [6], $ErNiSi_2$ [20], $CeRh_2Si_2$ [21] and $Tb_2Fe_3Si_5$ [22]. In contrast, the magnetic structures of $Tb_2Cr_2C_3$ and $Dy_2Cr_2C_3$ remain to be stable, since only one propagation vector and no further magnetic phase transitions could be observed. This may be rationalized by the fact that the Tb^{3+} and Dy^{3+} ions show usually a stronger single-ion anisotropy than Ho^{3+} and Er^{3+}. The magnetic order in intermetallic compounds is in fact a result of competing long-range interactions between the localized 4f moments via polarization of the conduction band (RKKY) and the influence of crystalline electric field (CEF).

Acknowledgements

We thank Dr. G. Höfer (Heraeus Quarzschmelze) for a valuable gift of silica tubes. We also acknowledge the support of the Deutsche

Forschungsgemeinschaft and the Fonds der Chemischen Industrie

References

[1] W. Jeitschko, M.H. Gerss, J. Less–Common Met. 116 (1986) 147.
[2] W. Jeitschko, R.K. Behrens, Z. Metallkd. 77 (1986) 788.
[3] W. Schäfer, W. Kockelmann, G. Will, J.K. Yakinthos, P.A. Kotsanidis, J. Alloys Compounds 250 (1997) 565.
[4] H. Onodera, N. Uchida, M. Ohashi, H. Yamauchi, Y. Yamaguchi, N. Sato, J. Magn. Magn. Mater. 137 (1994) 35.
[5] Y. Koshikawa, H. Onodera, M. Kosaka, H. Yamauchi, M. Ohashi, Y. Yamaguchi, J. Magn. Magn. Mater. 173 (1997) 72.
[6] J.K. Yakinthos, P.A. Kotsanidis, W. Schäfer, W. Kockelmann, G. Will, W. Reimers, J. Magn. Magn. Mater. 136 (1994) 327.
[7] H. Onodera, M. Ohashi, H. Amanai, S. Matsuo, H. Yamauchi, Y. Yamaguchi, S. Funahashi, Y. Morii, J. Magn. Magn. Mater. 149 (1995) 287.
[8] K. Zeppenfeld, R. Pöttgen, M. Reehuis, W. Jeitschko, R.K. Behrens, J. Phys. Chem. Solids 54 (1993) 257.
[9] M. Reehuis, K. Zeppenfeld, W. Jeitschko, E. Ressouche, J. Alloys Compounds 209 (1994) 217.
[10] M. Reehuis, M. Gerdes, W. Jeitschko, B. Ouladdiaf, N. Stüsser, J. Magn. Magn. Mater. 195 (1999) 657.
[11] M. Reehuis, N. Stüsser, K. Zeppenfeld, W. Jeitschko, Acta Crystallogr. A 52 (1996) C-498.
[12] M. Atoji, J. Chem. Phys. 54 (1971) 3504.
[13] M. Atoji, J. Chem. Phys. 74 (1981) 1893.
[14] J. Rodriguez-Carvajal, FullProf: a program for Rietveld refinement and pattern matching analysis, Abstract of the Satellite Meeting on Powder Diffraction of the XV Congress of the IUCr, Toulouse, 1990, p. 127.
[15] V.F. Sears, in: A.J.C. Wilson (Ed.), International Tables of Crystallography, Vol. C, Kluwer, Dordrecht, 1992, p. 383.
[16] P.J. Brown, in: A.J.C. Wilson (Ed.), International Tables of Crystallography, Vol. C, Kluwer, Dordrecht, 1992, p. 391.
[17] J.E. Greedan, V.U.S. Rao, J. Solid State Chem. 6 (1973) 387.
[18] J.E. Greedan, V.U.S. Rao, J. Solid State Chem. 8 (1973) 368.
[19] A. Szytula, J. Leciejewicz, in: K.A. Gschneidner Jr., L. Eyring (Eds.), Handbook on the Physics and Chemistry of Rare Earths, North-Holland, Amsterdam, 1989, pp. 133–211.
[20] P. Schobinger-Papamantellos, K.H.J. Buschow, C. Wilkinson, F. Fauth, C. Ritter, J. Magn. Magn. Mater. 189 (1998) 214.
[21] B.H. Grier, J.M. Lawrence, V. Murgai, R.D. Parks, Phys. Rev. B 29 (1984) 2664.
[22] A.R. Moodenbaugh, D.E. Cox, H.F. Braun, Phys. Rev. B 25 (1982) 4702.